**A SEMI-INFINITE HIGHER-ORDER DISPLACEMENT
DISCONTINUITY METHOD AND ITS APPLICATION TO THE
QUASISTATIC ANALYSIS
OF RADIAL CRACKS PRODUCED BY BLASTING**

Hasan Hosseini_Nasab and Mohammad Fatehi Marji

A SEMI-INFINITE HIGHER-ORDER DISPLACEMENT DISCONTINUITY METHOD AND ITS APPLICATION TO THE QUASISTATIC ANALYSIS OF RADIAL CRACKS PRODUCED BY BLASTING

HASAN HOSSEINI_NASAB AND MOHAMMAD FATEHI MARJI

We introduce a higher-order indirect boundary element method in a traction-free half-plane known as semi-infinite displacement discontinuity method. The method is modified to use the linear elastic fracture mechanics principles for radial crack analysis in brittle materials like rocks. In this numerical method there is no need to discretize the traction-free boundary of the half-plane into higher-order elements thus decreasing the number of elements without affecting the accuracy of the solution to the desired problems. The use of higher-order elements increases the accuracy so that it is possible to discretize both the boundary of the body and radial cracks by the same higher-order elements, therefore there may be no need to use the more complicated hybrid methods. A special crack tip element is added for each crack tip to increase the accuracy of displacement discontinuities near the crack ends due to their singularities. Based on the brittle behavior of most rocks, linear elastic fracture mechanics principles have been used to find the fracture mechanics parameters (mode-I and mode-II mixed mode stress intensity factors) of radial cracks occurring in common blasting operations. Arbitrary fracture criteria can be implemented in this code, but here a simple maximum tangential stress criterion is used to predict the angle of deviation (initiation) of radial cracks. Although this code is specially designed to include the traction-free half-plane problems, it is somewhat comprehensive so that any number of radial cracks with any length in the finite, infinite and semi-infinite planes can be treated easily. The validity of the method is proved by solving simple examples and some previously solved problems in the literature.

1. Introduction

In this work we formulate a new higher-order semi-infinite displacement discontinuity method and use it to analyze a number of crack problems. This method assumes linear or quadratic variation of displacement discontinuity in a semi-infinite body with a traction-free surface. It is based on the use of two or three collocation points (for linear or quadratic displacement discontinuity variation, respectively) over a two-element or three-element "patch" centered at the source element. This method is suitable for solving some fracture mechanics problems, because the special crack tip elements can easily be incorporated in this algorithm. We adopt the hybrid element formulation: higher-order elements are used for the discretization of all boundaries excluding the crack tips, and a special crack tip element is used for discretization of the crack ends.

Fracture mechanics has been suggested as a possible tool for solving a variety of rock engineering problems, such as rock cutting, hydrofracturing, explosive fracturing, rock stability, etc. In 1957, Irwin modified the basic theory of fracture of Griffith [1925] and introduced the important parameters called

---

Keywords: DDM, half-plane problems, higher-order elements, radial cracks, LEFM.

stress intensity factors (SIFs), to express the stress and displacement fields near the crack tip. Three SIFs, denoted by K_I, K_{II} and K_{III}, were introduced, corresponding to three basic fracture modes: opening or tensile (mode I), sliding or shearing (mode II) and tearing (mode III).

Recently linear elastic fracture mechanics (LEFM) principles have been widely used in rock fracture mechanics (RFM) [Rossmanith 1983; Whittaker et al. 1992; Aliabadi 1998]. Based on LEFM principles, a superposition of the three fracture modes describes the general case of loading called mixed mode loading. For a given cracked body under a certain type of loading, the SIFs are known and the displacements and stresses near the crack tip are accordingly determined. Therefore, the problem of LEFM reduces to the determination of the crack tip SIFs. Hybrid element formulations have been used in the literature of fracture mechanics [Guo et al. 1992; Scavia 1992; Scavia 1995; Tan et al. 1996; Carpinteri and Yang 1997; Bobet 2001; Shen et al. 2004]. Because of their complexity, fracture mechanics problems are usually solved numerically by using the complicated hybrid methods [Scavia 1995; Stephansson 2002]. Due to brittle behavior of most rocks, the linear elastic fracture mechanics principles have been used to find the fracture mechanics parameters; that is, the (I and II) mixed-mode stress intensity factors (SIFs) of radial cracks occur in the common blasting operations. For the prediction of crack initiation and its angle of deviation the maximum tangential stress criterion introduced in [Erdogan and Sih 1963], is used which compares the computed SIFs with the fracture toughness (material properties like yield strength) that should be obtained experimentally [Huang and Wang 1985; Ouchterlony 1988; Stephansson et al. 2001; Backers et al. 2004; Shen et al. 2004]. A general numerical modeling for quasistatic crack analysis in semi-infinite plane is given and as a practical problem, the radial cracks around the blast holes are numerically analyzed. Any number of blast holes with any gas pressurization ratios along the emanating cracks can be studied by this model. Suitable normal gas pressurization ratios along the radial cracks are used, to solve the problem. As it was expected, the radial crack propagation takes place under tension (Mode I or opening mode of fracture), which is mainly responsible for rock blasting [Ouchterlony 1983].

2. Higher order (linear and quadratic elements) displacement discontinuity in a half-plane

General solutions and higher-order elements. Many boundary-value problems are set in traction-free half-spaces. Here we consider a two-dimensional traction-free half-plane. To implement the higher-order displacement discontinuity elements numerically, we need the analytical solution to the problem of a constant displacement discontinuity D_i integrated over a line element along the x-axis in an infinite elastic solid Crouch [1976] showed that the general solution to this problem, over a line element of length $2a$, can be expressed in terms of two harmonic functions $f(x, y)$ and $g(x, y)$ of x and y, in which the displacements are

$$
\begin{aligned}
u_x &= \left(2(1-\nu)f_{,y} - yf_{,xx}\right) + \left(-(1-2\nu)g_{,x} - yg_{,xy}\right), \\
u_y &= \left((1-2\nu)f_{,x} - yf_{,xy}\right) + \left(2(1-\nu)g_{,y} - yg_{,yy}\right)
\end{aligned}
\tag{1}
$$

and the stresses are

$$
\begin{aligned}
\sigma_{xx} &= 2G_s(2f_{,xy} + yf_{,xyy}) + 2G_s(g_{,yy} + yg_{,yyy}), \\
\sigma_{yy} &= 2G_s(-yf_{,xyy}) + 2G_s(g_{,yy} - yg_{,yyy}), \\
\sigma_{xy} &= 2G_s(2f_{,yy} + yf_{,yyy}) + 2G_s(-yg_{,xyy}),
\end{aligned}
\tag{2}
$$

where $f_{,x} = \partial f\, \partial x$ and so on.

Shou and Crouch [1995] proposed a new higher-order displacement discontinuity method for solving plane elasticity problems, exploiting the use of quadratic elements for analysis of crack problems in infinite bodies. In this paper the same kind of the higher-order displacement discontinuity elements is used for the analysis of crack problems in semi-infinite bodies, but both linear and quadratic elements are considered. The general higher-order expression of harmonic functions $f(x, y)$ and $g(x, y)$ can be rearranged as

$$f(x, y) = \frac{-1}{4\pi(1 - \nu)} \sum_{j=1}^{k} D_x^j F_j(I_{j-1}), \quad g(x, y) = \frac{-1}{4\pi(1 - \nu)} \sum_{j=1}^{k} D_y^j F_j(I_{j-1}). \tag{3}$$

Here k ranges over 1, 2 for linear elements and over 1, 2, 3 for quadratic elements. Similarly, the higher-order displacement discontinuity $D_i(\varepsilon)$ can be expressed as

$$D_i(\varepsilon) = \sum_{j=1}^{k} N_j(\varepsilon) D_i^j \quad \text{with } k \text{ as above and } i = x, y. \tag{4}$$

The displacement discontinuity using linear elements is based on analytical integration of linear collocation shape functions over collinear, straight-line displacement discontinuity elements. Figure 1a shows the linear displacement discontinuity distribution, which can be written as

$$D_i(\varepsilon) = N_1(\varepsilon) D_i^1 + N_2(\varepsilon) D_i^2, \quad i = x, y, \tag{5}$$

where D_i^1 and D_i^2 are the linear nodal displacement discontinuities and

$$N_1(\varepsilon) = -(\varepsilon - a_1)/2a_1, \qquad N_2(\varepsilon) = (\varepsilon + a_1)/2a_1 \tag{6}$$

are the linear collocation shape functions using $a_1 = a_2$. A linear element has two nodes, which are at the centers of its two equal subelements (Figure 1a).

Similarly, the quadratic element displacement discontinuity is based on the analytic integration of quadratic collocation shape functions over collinear, straight-line displacement discontinuity elements. Figure 1b shows the quadratic displacement discontinuity distribution, which can be written as

$$D_i(\varepsilon) = N_1(\varepsilon) D_i^1 + N_2(\varepsilon) D_i^2 + N_3(\varepsilon) D_i^3, \quad i = x, y, \tag{7}$$
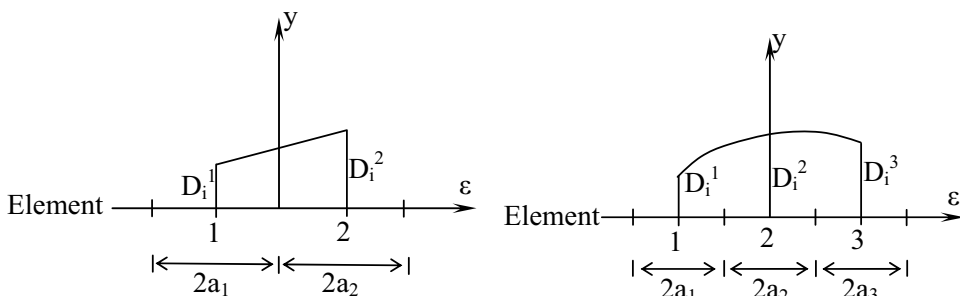

Figure 1. Linear (left) and quadratic (right) collocations for the higher-order displacement discontinuity elements.

where D_i^1, D_i^2, and D_i^3 are the quadratic nodal displacement discontinuities and

$$N_1(\varepsilon) = \varepsilon(\varepsilon - 2a_1)/8a_1{}^2, \quad N_2(\varepsilon) = -(\varepsilon^2 - 4a_1^2)/4a_1{}^2, \quad N_3(\varepsilon) = \varepsilon(\varepsilon + 2a_1)/8a_1{}^2 \tag{8}$$

are the quadratic collocation shape functions using $a_1 = a_2 = a_3$. A quadratic element has three nodes, at the centers of its three equal subelements (Figure 1b).

Considering a linear variation for $D_i(\varepsilon)$ as given in (5), the common function F_j in (3) is defined as

$$F_j(I_0, I_1) = \int N_j(\varepsilon) \ln\big((x - \varepsilon) + y^2\big)^{1/2} d\varepsilon, \quad j = 1, 2. \tag{9}$$

Here the integrals I_0 and I_1 are expressed as

$$I_0(x, y) = \int_{-a}^{a} \ln\big((x - \varepsilon)^2 + y^2\big)^{1/2} d\varepsilon = y(\theta_1 - \theta_2) - (x - a)\ln(r_1) + (x + a)\ln r_2 - 2a \tag{10}$$

$$I_1(x, y) = \int_{-a}^{a} \varepsilon \ln\big((x - \varepsilon)^2 + y^2\big)^{1/2} d\varepsilon = xy(\theta_1 - \theta_2) + \tfrac{1}{2}(y^2 - x^2 + a^2)\ln\frac{r_1}{r_2} - ax, \tag{11}$$

where we have defined

$$\theta_1 = \arctan\frac{y}{x - a}, \quad \theta_2 = \arctan\frac{y}{x + a}, \quad r_1 = \big((x - a)^2 + y^2\big)^{1/2}, \quad r_2 = \big((x + a)^2 + y^2\big)^{1/2}. \tag{12}$$

Similarly, considering a quadratic variation for $D_i(\varepsilon)$ as given in Equation (7), the common function F_j in (3) is defined as

$$F_j(I_0, I_1, I_2) = \int N_j(\varepsilon) \ln\big((x - \varepsilon) + y^2\big)^{1/2} d\varepsilon, \quad j = 1, 2, 3, \tag{13}$$

where I_0 and I_1 are as in (5) and (13) and

$$I_2(x, y) = \int_{-a}^{a} \varepsilon^2 \ln\big((x - \varepsilon)^2 + y^2\big)^{1/2} d\varepsilon \tag{14}$$

$$= \frac{y}{3}(3x^2 - y^2)(\theta_1 - \theta_2) + \tfrac{1}{3}(3xy^2 - x^3 + a^3)\ln(r_1) - \tfrac{1}{3}(3xy^2 - x^3 - a^3)\ln(r_2) - \frac{2a}{3}\Big(x^2 - y^2 + \frac{a^2}{3}\Big).$$

A routine computation yields the partial derivatives of the integrals I_0, I_1 and I_2 with respect to x and y. These derivatives are needed in the calculation of displacements and stresses in semi-infinite plane problems. As an example,

$$I_{2,yyyy} = -2\Big(\frac{(x - a)}{r_1^2} - \frac{(x + a)}{r_2^2}\Big) + 2a\Big(\frac{(x - a)^2 - y^2}{r_1^4} + \frac{(x + a)^2 - y^2}{r_2^4}\Big)$$

$$-2a^2\Big(\frac{(x - a)^2(r_1^2 - 4y^2)}{r_1^6} - \frac{(x + a)^2(r_2^2 - 4y^2)}{r_2^6}\Big),$$

where r_1, r_2, θ_1, and θ_2 are defined in (12).
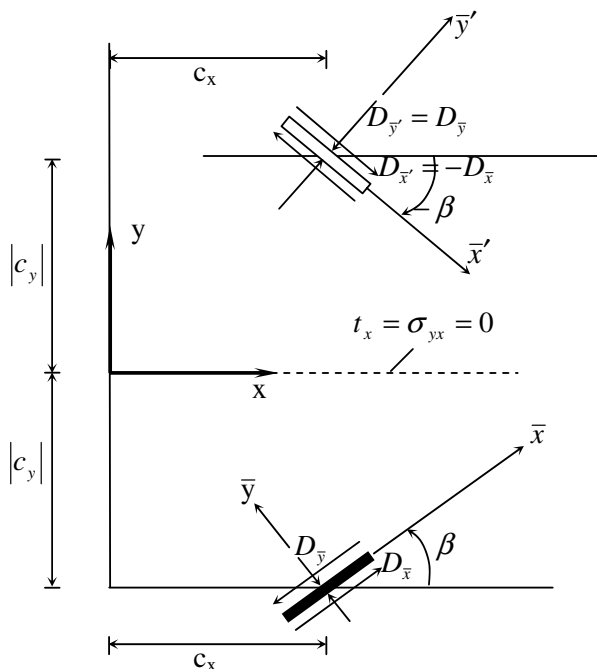
Figure 2. The actual and image displacement discontinuities in half-plane $y \leq 0$.

Half-plane solution. The analytical solution to a constant element displacement discontinuity over the line segment $|x| \leq a$, $y = 0$ in the semi-infinite region $y \leq 0$ is found in [Crouch and Starfield 1983] using the method of images to be

$$u_i = u_i^A + u_i^I + u_i^S, \quad \sigma_{ij} = \sigma_{ij}^A + \sigma_{ij}^I + \sigma_{ij}^S, \tag{15}$$

where the displacements and stresses due to the actual displacement discontinuity are denoted by a superscript A, those due to its image by I and those resulting from the supplementary solution by S.

Based on the local $\bar{x}$, $\bar{y}$ coordinates and the image local $\bar{x}'$, $\bar{y}'$ coordinates shown in Figure 2, the displacements and stresses given in (15) can be obtained in global x, y coordinates by using the coordinate, displacement and stress transformation rules explained in [Crouch and Starfield 1983]. Considering the geometry shown in Figure 2, the displacements and stresses due to actual displacement discontinuities can be written directly from (1) and (2). The local $\bar{x}$, $\bar{y}$ coordinates are related to the global x, y coordinates by the transformation formulas

$$\begin{aligned} \bar{x} &= (x - c_x)\cos\beta + (y - c_y)\sin\beta, \\ \bar{y} &= -(x - c_x)\sin\beta + (y - c_y)\cos\beta. \end{aligned} \tag{16}$$

Denoting the common potential function $F_j(x, y)$ by $F_j^A(\bar{x}, \bar{y}) = F_{j1}^A$ and its derivatives by $F_{j,\bar{x}}^A = F_{j2}^A$, $F_{j,\bar{y}}^A = F_{j3}^A$, $F_{j,\overline{xy}}^A = F_{j4}^A$, $F_{j,\overline{xx}}^A = -F_{j,\overline{yy}}^A = F_{j5}^A$, $F_{j,\overline{xyy}}^A = F_{j6}^A$, $F_{j,\overline{yyy}}^A = F_{j7}^A$, for the actual displacement

discontinuities, the actual displacements in terms of the global x, y coordinates are given by

$$u_x^A = \frac{-1}{4\pi(1-\nu)} \sum_{J=1}^{3} \Big(\big(-(1-2\nu)\sin\beta F_{j2}^A + 2(1-\nu)\cos\beta F_{j3}^A + \bar{y}(\sin\beta F_{j4}^A - \cos\beta F_{j5}^A)\big)D_{\bar{x}}^j$$
$$+ \big(-(1-2\nu)\cos\beta F_{j2}^A - 2(1-\nu)\sin\beta F_{j3}^A - \bar{y}(\cos\beta F_{j4}^A + \sin\beta F_{j5}^A)\big)D_{\bar{y}}^j \Big),$$

$$u_y^A = \frac{-1}{4\pi(1-\nu)} \sum_{J=1}^{3} \Big(\big((1-2\nu)\cos\beta F_{j2}^A + 2(1-\nu)\sin\beta F_{j3}^A - \bar{y}(\cos\beta F_{j4}^A + \sin\beta F_{j5}^A)\big)D_{\bar{x}}^j$$
$$+ \big(-(1-2\nu)\sin\beta F_{j2}^A + 2(1-\nu)\cos\beta F_{j3}^A - \bar{y}(\sin\beta F_{j4}^A - \cos\beta F_{j5}^A)\big)D_{\bar{y}}^j \Big), \quad (17)$$

and the actual stresses by

$$\sigma_{xx}^A = \frac{-2G}{4\pi(1-\nu)} \sum_{j=1}^{3} \Big(2\cos^2\beta F_{j4}^A + \sin 2\beta F_{j5}^A + \bar{y}(\cos 2\beta F_{j6}^A - \sin 2\beta F_{j7}^A)D_{\bar{x}}^j$$
$$+ \big(-F_{j5}^A + \bar{y}(\sin 2\beta F_{j6}^A + \cos 2\beta F_{j7}^A)\big)D_{\bar{y}}^j \Big),$$

$$\sigma_{yy}^A = \frac{-2G}{4\pi(1-\nu)} \sum_{j=1}^{3} \Big(\big(2\sin^2\beta F_{j4}^A - \sin 2\beta F_{j5}^A - \bar{y}(\cos 2\beta F_{j6}^A + \sin 2\beta F_{j7}^A)\big)D_{\bar{x}}^j$$
$$+ \big(-F_{j5}^A - \bar{y}(\sin 2\beta F_{j6}^A + \cos 2\beta F_{j7}^A)\big)D_{\bar{y}}^j \Big),$$

$$\sigma_{xy}^A = \frac{-2G}{4\pi(1-\nu)} \sum_{j=1}^{3} \Big(\big(\sin 2\beta F_{j4}^A - \cos 2\beta F_{j5}^A + \bar{y}(\sin 2\beta F_{j6}^A + \cos 2\beta F_{j7}^A)\big)D_{\bar{x}}^j$$
$$- \bar{y}(\cos 2\beta F_{j6}^A - \sin 2\beta F_{j7}^A)D_{\bar{y}}^j \Big). \quad (18)$$

The displacements and stresses due to the image displacement discontinuity can be expressed in term of a single function $F_j^I(\bar{x}', \bar{y}')$ in which the image local $\bar{x}', \bar{y}'$ coordinates (as shown in Figure 2) are related to the x, y coordinates by the transformation formula

$$\bar{x}' = (x - c_x)\cos\beta - (y + c_y)\sin\beta,$$
$$\bar{y}' = (x - c_x)\sin\beta + (y + c_y)\cos\beta, \quad (19)$$

which is obtained by replacing c_y and β in (16) by c_y and $-\beta$.

It can be shown that the supplementary solution for the displacements and stresses can be expressed in term of the function $F_j^I(\bar{x}', \bar{y}')$ and its derivatives. The final expressions for the combined displacements $u_i^I + u_i^S$ and stresses $\sigma_{ij}^I + \sigma_{ij}^S$ as given in the Appendix.

The displacement discontinuity functions $D_i(\varepsilon)$ in (4) can be used either in a constant element form or in a higher-order element form as follows, to solve the displacements and stresses of (1), (2) and (15). Two degrees of freedom are used for each node at the center of each element. Crawford and Curran [1982] have developed a higher-order displacement discontinuity for linear and quadratic elements using four and six degrees of freedom respectively. Shou and Crouch [1995] have introduced a new higher-order displacement discontinuity for two-dimensional infinite plane problems using only two degrees of freedom for each element while still preserving the advantages of the approach in [Crawford and Curran 1982].

In this study, Shou and Crouch's approach is extended and modified for both linear and quadratic displacement discontinuity variations (the original formulation covers only quadratic displacement variations in infinite plane problems) in order to solve the half-plane boundary-value problems with traction-free surfaces. For linear and quadratic displacement variations, the interpolation of displacement values over two- and three-element patches, respectively, is the basis of our formulation (recall Figure 1).

The general solution to plane elasticity problems involves two types of boundary conditions: the stress boundary conditions $\sigma_s{}^i = (\sigma_s{}^i)_0$, $\sigma_n{}^i = (\sigma_n{}^i)_0$ and the displacement boundary conditions $u_s{}^i = (u_s{}^i)_0$, $u_n{}^i = (u_n{}^i)_0$. In these equations the right-hand sides stand for the given boundary values of the stresses and displacements for the local s and n coordinates (that is, the same as the local $\bar{x}$, $\bar{y}$ coordinates shown in Figure 2) defining at the center of each two-element patch (linear variation) or three-element patch (quadratic variation). Finally, then, we obtain a system of $2 \times 2N$ or $2 \times 3N$ algebraic equations in as many unknown displacement discontinuity components:

$$b_s^i = \sum_{j=1}^{N} C_{ss}(i, j) D_s^j + \sum_{j=1}^{N} C_{sn}(i, j) D_n^j, \quad b_n^i = \sum_{j=1}^{N} C_{ns}(i, j) D_s^j + \sum_{j=1}^{N} C_{nn}(i, j) D_n^j, \quad i = 1, N. \quad (20)$$

The quantities b_s^i and b_n^i stand for the known boundary values of stress and displacement, and $C_{ss}(i, j)$, etc., are the corresponding influence coefficients [Crouch and Starfield 1983]. For the solution of cracked body problems in half-planes with traction-free surfaces, we developed two computer programs: SIDDLCR for semi-infinite displacement discontinuity method using linear displacement discontinuity elements for crack analysis and SIDDQCR for semi-infinite displacement discontinuity method using quadratic displacement discontinuity elements for crack analysis. Since the solution of the infinite plane case is part of the solution of the half-plane problems (i.e., the actual solution part given in (17) and (18)), these two computer codes can actually solve general elasticity problems in finite, infinite and semi-infinite planes.

3. Crack tip element formulation and stress intensity factor computation

Consider a body of arbitrary shape with a crack of arbitrary size, subjected to arbitrary tensile and shear loadings (mode-I and mode-II loading). The stresses and displacements near the crack tip are given in [Rossmanith 1983; Whittaker et al. 1992] and other textbooks; but since we use the displacement discontinuity method here we need the formulations given for the SIFs K_I and K_{II} in terms of the normal and shear displacement discontinuities [Whittaker et al. 1992; Scavia 1995]:

$$K_I = \frac{G}{4(1-\nu)} \left(\frac{2\pi}{a}\right)^{1/2} D_y(a), \qquad K_{II} = \frac{G}{4(1-\nu)} \left(\frac{2\pi}{a}\right)^{1/2} D_x(a). \quad (21)$$

Due to the singularity variations $1/\sqrt{r}$ and $\sqrt{r}$ for the stresses and displacements in the vicinity of the crack tip the accuracy of the displacement discontinuity method decreases, and usually a special treatment of the crack at the tip is necessary. A special crack tip element which already has been introduced in literature (see [Crouch and Starfield 1983], for example) is used here to represent the singularity. Using a special crack tip element of length $2a$ as shown in Figure 3, we obtain the parabolic displacement
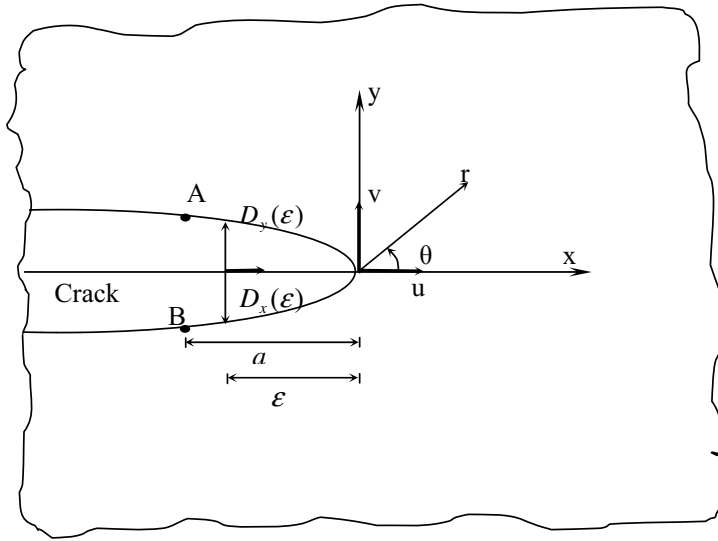
Figure 3. Displacement correlation technique for the special crack tip element.

discontinuity variations along this element as

$$D_i(\varepsilon) = D_i(a)(\varepsilon/a)^{1/2}, \quad i = x, y, \tag{22}$$

where ε is the distance from crack tip and $D_y(a)$ and $D_x(a)$ are the opening (normal) and sliding (shear) displacement discontinuities at the center of special crack tip element.

The potential functions $f_C(x, y)$ and $g_C(x, y)$ for the crack tip element can be expressed as

$$f_C(x, y) = \frac{-1}{4\pi(1-\nu)} \int_{=a}^{a} \frac{D_x(a)}{a^{1/2}} \varepsilon^{1/2} \ln\big((x-\varepsilon)^2 + y^2\big)^{1/2} d\varepsilon,$$
$$g_C(x, y) = \frac{-1}{4\pi(1-\nu)} \int_{=a}^{a} \frac{D_y(a)}{a^{1/2}} \varepsilon^{1/2} \ln\big((x-\varepsilon)^2 + y^2\big)^{1/2} d\varepsilon. \tag{23}$$

These functions have a common integral of the form

$$I_C = \int_0^{2a} \varepsilon^{1/2} \ln\big((x-\varepsilon)^2 + y^2\big)^{1/2} d\varepsilon. \tag{24}$$

The derivatives of this integral, which are used in calculation of the crack tip displacement discontinuities in semi-infinite plane problems, are easily computed:

$$I_{c,x} = \int_0^{2a} \frac{\varepsilon^{1/2}(x-\varepsilon)}{(x-\varepsilon)^2 + y^2} d\varepsilon = xA_1 - A_2, \qquad I_{c,y} = \int_0^{2a} \frac{\varepsilon^{1/2}y}{(x-\varepsilon)^2 + y^2} d\varepsilon = yA_1,$$

where we have introduced

$$A_1 = \frac{1}{\rho}\left(\frac{1}{2}\left(\cos\varphi - \frac{x}{y}\sin\varphi\right)\ln\frac{2a - 2\sqrt{2a}\rho\cos\varphi + \rho^2}{2a + 2\sqrt{2a}\rho\cos\varphi + \rho^2} + \left(\sin\varphi + \frac{x}{y}\cos\varphi\right)\arctan\left(\frac{2\sqrt{2a}\rho\sin\varphi}{\rho^2 - 2a}\right)\right),$$

$$A_2 = \rho\left(\frac{1}{2}\left(\cos\varphi + \frac{x}{y}\sin\varphi\right)\ln\frac{2a - 2\sqrt{2a}\rho\cos\varphi + \rho^2}{2a + 2\sqrt{2a}\rho\cos\varphi + \rho^2} + \left(\sin\varphi + \frac{x}{y}\cos\varphi\right)\arctan\left(\frac{2\sqrt{2a}\rho\sin\varphi}{\rho^2 - 2a}\right)\right),$$

with $\rho = (x^2 + y^2)^{1/4}$ and $\varphi = \frac{1}{2}\arctan(y/x)$. Moreover,

$$I_{c,xy} = yA_{1,x}, \qquad I_{c,xyy} = A_{1,x} + yA_{1,xy}, \qquad I_{c,xyyy} = 2A_{1,xy} + yA_{1,xyy},$$

$$I_{c,yy} = A_1 + yA_{1,y} = -I_{c,xx}, \qquad I_{c,yyy} = 2A_{1,y} + yA_{1,yy}, \qquad I_{c,yyyy} = 3A_{1,yy} + yA_{1,yyy}.$$

4. Crack initiation and direction of its propagation

Several mixed mode fracture criteria are well known from the literature [Ingraffea 1981; 1987; Huang and Wang 1985; Zipf and Bieniawski 1989; Ouchterlony 1988; Stephansson et al. 2001; Rao et al. 2003; Backers et al. 2004; Shen et al. 2004], any of them can be applied to crack analysis problems using this model. In this study as the blast hole radial cracks are mostly in opening mode case, the simple maximum tangential stress criterion or σ-criterion is used here to predict the angle of crack initiation. This criterion is a mixed mode fracture criterion which is widely used and well fitted with the experimental results [Ingraffea 1983; Broek 1989; Guo et al. 1992; Carpinteri and Yang 1997].

Based on this criterion the crack tip will start propagating when

$$\cos\frac{\theta_0}{2}\left(K_I\cos^2\frac{\theta_0}{2} - \frac{3}{2}K_{II}\sin\frac{\theta_0}{2}\right) = K_{IC}, \tag{25}$$

where K_{IC} is the mode-I fracture toughness of the material and θ_0 is the propagation angle. The latter value corresponding to the crack tip should satisfy the condition

$$K_I\sin\theta_0 + K_{II}(3\cos\theta_0 - 1) = 0. \tag{26}$$

5. Verification of higher-order semi-infinite displacement discontinuity

Verification of this method is made through the solution of simple example problems. We first take a center slant crack in an infinite body, as shown in Figure 4. The slant angle, β, changes counterclockwise from the x-axis, and the tensile stress $\sigma = 10$ MPa acts parallel to the x-axis. A half crack length $b = 1$ meter, modulus of elasticity $E = 10$ GPa, Poisson's ratio $\nu = 0.2$, fracture toughness $K_{IC} = 2$ MPa$\sqrt{}$ m are assumed. The analytical solution of the first and second mode stress intensity factors K_I and K_{II} for the infinite body problem are given as (see [Guo et al. 1990; Whittaker et al. 1992])

$$K_I = \sigma(\pi b)^{1/2}\sin^2\beta \qquad \Longrightarrow \qquad \frac{K_I}{\sigma\sqrt{\pi b}} = \sin^2\beta,$$

$$K_{II} = \sigma(\pi b)^{1/2}\sin\beta\cos\beta \implies \frac{K_{II}}{\sigma\sqrt{\pi b}} = \sin\beta\cos\beta. \tag{27}$$
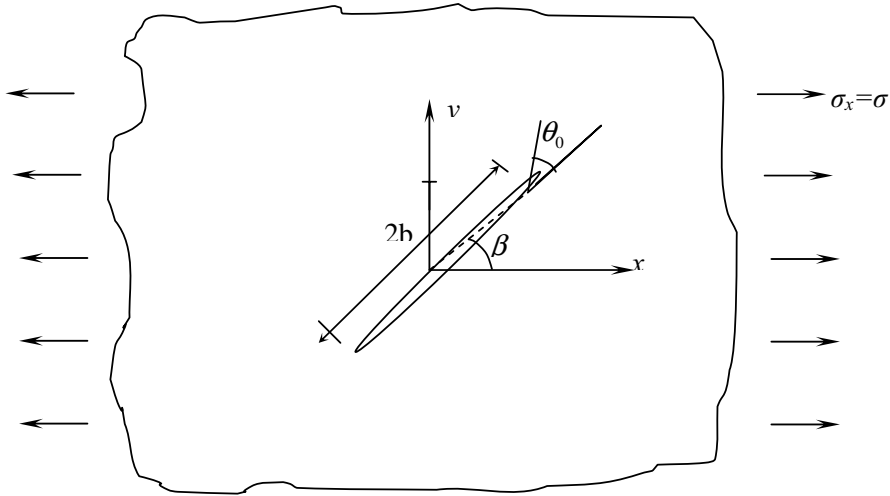
Figure 4. Center slant cracks in an infinite body under far-field tension.

The normalized mixed mode stress intensity factors, $K_I/(\sigma\sqrt{\pi b})$ and $K_{II}/(\sigma\sqrt{\pi b})$, are obtained analytically for different crack inclination from Equations (27), and numerically by means of the two software programs SIDDLCR and SIDDQCR (page 445), using a total of 98 nodes and a crack tip length equal to one-tenth the half crack length — that is, an L/b ratio of 0.1. Some of the results obtained are tabulated in Table 1, and give an idea of the accuracy and usefulness of the programs.

To investigate the effect of the number of elements on accuracy, we solved numerically two problems, respectively with 45° and 30° slanted cracks, choosing $L/b = 0.1$ and a varying number of nodes. The normalized numerical results are given in Table 2. They show that using any number of nodes above 24 gives very accurate values for both SIDDLCR and SIDDQCR.

Angle β	$K_I/(\sigma\sqrt{\pi b})$			$K_{II}/(\sigma\sqrt{\pi b})$		
	Analytic	SIDDQCR	SIDDLCR	Analytic	SIDDQCR	SIDDLCR
10°	0.0302	0.0302	0.0309	0.1711	0.1711	0.1752
20°	0.1170	0.1171	0.1198	0.3214	0.3216	0.3292
30°	0.2500	0.2502	0.2561	0.4330	0.4334	0.4435
40°	0.4132	0.4135	0.4176	0.4924	0.4920	0.4977
50°	0.5868	0.5864	0.5932	0.4924	0.4921	0.4977
60°	0.7500	0.7495	0.7581	0.4330	0.4327	0.4369
70°	0.8830	0.8824	0.8926	0.3214	0.3212	0.3249
80°	0.9696	0.9692	0.9803	0.1711	0.1709	0.1713
90°	1.0000	0.9996	1.011	0.0000	0.0000	0.0000

Table 1. Analytical and numerical values of the normalized stress intensity factors for the slant center crack at different orientation from the loaded axis (x-axis), for $L/b = 0.1$ and 98 nodes.

Nodes	$K_I/(\sigma\sqrt{\pi b})$ (45°)		$K_I/(\sigma\sqrt{\pi b})$ (30°)		$K_{II}/(\sigma\sqrt{\pi b})$ (30°)	
	SIDDQCR	SIDDLCR	SIDDQCR	SIDDLCR	SIDDQCR	SIDDLCR
12	0.5116	0.5396	0.2558	0.2698	0.4431	0.4673
24	0.5014	0.5160	0.2507	0.2580	0.4342	0.4469
36	0.4999	0.5097	0.2500	0.2549	0.4330	0.4414
48	0.4997	0.5069	0.2499	0.2535	0.4327	0.4390
60	0.4997	0.5054	0.2498	0.2527	0.4327	0.4377
72	0.4997	0.5044	0.2498	0.2522	0.4327	0.4368
84	0.4998	0.5038	0.2499	0.2517	0.4328	0.4363
96	0.4998	0.5033	0.2499	0.2516	0.4328	0.4358
108	0.4999	0.5029	0.2499	0.2514	0.4328	0.4355
120	0.4999	0.5026	0.2499	0.2513	0.4329	0.4353

Table 2. Numerical values of the stress intensity factors for the 45° and 30° slant center cracks using varying number of nodes and $L/b = 0.1$.

Finally, to show the effect of the length of the crack tip element on the accuracy of the results, the same two problems are solved numerically using 98 nodes and different L/b ratios. The results are given in Table 3. We see that for any L/b ratio above 0.025, both programs give very accurate values.

Because of its simplicity, the center slant crack problem has been solved by various investigators such as Guo et al. [1990], who used constant element displacement discontinuity with a special crack tip element for angles 30°, 40°, 50°, 60°, 70° and 80°. These authors used a different fracture criterion for evaluating the crack initiation angle θ_0 and compared their results with the results obtained by other

L/b	$K_I/(\sigma\sqrt{\pi b})$ (45°)		$K_I/(\sigma\sqrt{\pi b})$ (30°)		$K_{II}/(\sigma\sqrt{\pi b})$ (30°)	
	SIDDQCR	SIDDLCR	SIDDQCR	SIDDLCR	SIDDQCR	SIDDLCR
0.025	0.5028	0.5166	0.2514	0.2614	0.4354	0.4467
0.050	0.5000	0.5072	0.2500	0.2536	0.4330	0.4393
0.075	0.4998	0.5045	0.2498	0.2523	0.4328	0.4369
0.100	0.4998	0.5033	0.2499	0.2516	0.4328	0.4358
0.125	0.4999	0.5026	0.2499	0.2513	0.4329	0.4352
0.150	0.5001	0.5021	0.2500	0.2511	0.4331	0.4349
0.175	0.5003	0.5019	0.2501	0.2510	0.4333	0.4347
0.200	0.5005	0.5018	0.2503	0.2509	0.4335	0.4346
0.225	0.5008	0.5018	0.2504	0.2509	0.4337	0.4346
0.250	0.5011	0.5019	0.2506	0.2510	0.4340	0.4347
0.275	0.5015	0.5021	0.2507	0.2510	0.4343	0.4348
0.300	0.5019	0.5023	0.2509	0.2512	0.4346	0.4350

Table 3. Numerical values of the stress intensity factors for the 45° and 30° slant center cracks using varying L/b ratios and 98 nodes.

| Angle β | θ_0, present work | | θ_0 as reported in [Guo et al. 1990] | | | |
	SIDDQCR	SIDDLCR	σ-criterion	S-criterion	Exper.	Numer.
30	60.00	60.00	60.2	63.5	62.4	67.0
40	55.65	55.65	55.7	56.7	55.1	59.0
50	50.29	50.29	50.2	49.5	51.1	51.0
60	43.22	43.22	43.2	41.9	43.1	41.0
70	33.26	33.26	33.2	31.8	30.7	29.0
80	18.91	18.91	19.3	18.5	17.3	15.0

Table 4. Crack initiation angle θ_0 obtained by different methods for the center slant crack problem.

researchers using different fracture theories. Table 4 compares the results obtained for crack initiation angle θ_0 with SIDDLCR and SIDDQCR, using the maximum tangential stress theory proposed by Erdogan and Sih [1963], and the results obtained by other methods as given by Guo et al. The numerical results obtained here are very close to those predicted by the σ-criterion.

For the verification of the semi-infinite higher-order displacement discontinuity method, the problem of a 45° slant crack with different depths (C/b ratio) from the free surface of the half-plane is considered. This is the problem shown in Figure 5, where $C = C_y$ is the depth at the center of the slant crack from the free surface of the half-plane as shown in Figure 3.

The normalized stress intensity factors $K_I/(\sigma\sqrt{\pi b})$ and $K_{II}/(\sigma\sqrt{\pi b})$ of the upper and lower crack tips were obtained using SIDDQCR. The numerical results for the 45° crack are given in Table 5, where
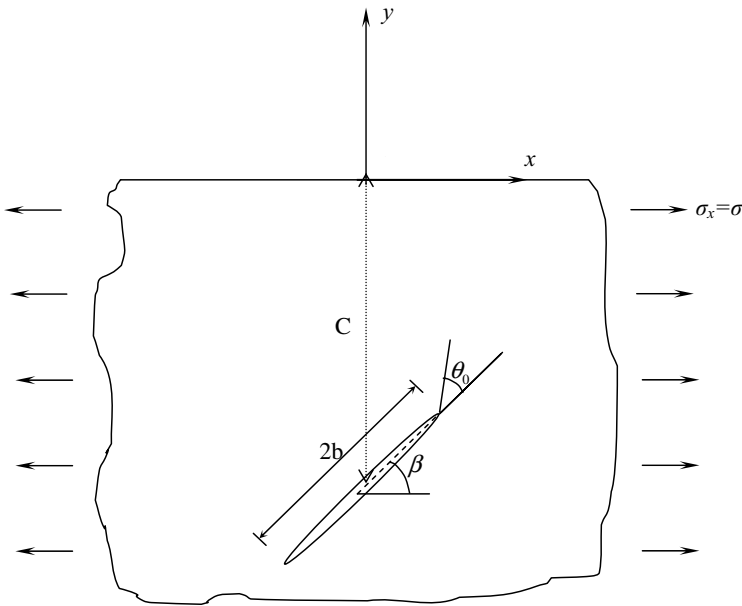

Figure 5. Slant cracks in a semi-infinite body under far field tension.

C/b ratio	$K_I/(\sigma\sqrt{\pi b})$		$K_{II}/(\sigma\sqrt{\pi b})$	
	Upper Tip	Lower Tip	Upper Tip	Lower Tip
1	0.6147	0.5278	0.4603	0.5530
2	0.5115	0.5067	0.4669	0.4957
3	0.4989	0.4996	0.4785	0.4907
4	0.4959	0.4971	0.4841	0.4905
5	0.4951	0.4961	0.4874	0.4911
6	0.4950	0.4958	0.4895	0.4919
7	0.4951	0.4958	0.4909	0.4927
8	0.4953	0.4959	0.4920	0.4930
9	0.4956	0.4960	0.4929	0.4938
10	0.4958	0.4962	0.4935	0.4943

Table 5. Normalized stress intensity factors $K_I/(\sigma\sqrt{\pi b})$ and $K_{II}/(\sigma\sqrt{\pi b})$ of the upper and lower crack tips for a 45 degrees inclined crack in a semi-infinite body with different C/b ratios, using 98 nodes and $L/b = 0.1$.

we have used a total of 98 nodes (including the two crack tip elements) and an L/b ratio of 0.1. The table shows that as the crack becomes very close to the free surface of the half-plane, the mode-I stress intensity factor K_I of the upper crack tip (the one nearer the free surface) increases more rapidly compared to that of the lower tip, but the mode-II stress intensity factor K_{II} decreases. The analytical solution for the 45° center slant crack in an infinite plate gives $K_I/(\sigma\sqrt{\pi b}) = K_{II}/(\sigma\sqrt{\pi b}) = 0.5$, and as can be seen from the table, the numerical values tend to this analytical value as the depth C increases to infinity.

6. Numerical analysis of radial cracks in blasting

Radial crack propagation in blasting operations is a complicated and interesting phenomenon. The initiation and propagation mechanisms have been investigated in [Ingraffea 1983; Mortazavi and Katsabanis 2001; Cho et al. 2004]. Generally, two forms of radial crack analysis have been used: dynamic crack analysis (considering stress wave and/or gas pressurization theories) and quasistatic crack analysis (considering only gas pressurization theory); see [Kutter and Fairhurst 1971; Courtesen 1979; Ash 1985; Donzé et al. 1997; Cho et al. 2004]. Dynamic crack analysis is far beyond our scope; instead we briefly consider quasistatic radial crack analysis due to gas pressurization, to show the effectiveness of the present model for solving some crack problems occurring in rock fracture mechanics. Analytical solutions of the radial crack propagation in an infinite elastic rock have been discussed in the literature; see [Ouchterlony 1983; Whittaker et al. 1992] and references therein. Ouchterlony has extensively analyzed various load configurations in relation to rock blasting and determined the stress intensity factors for them by using the conformal mapping method. This has provided valuable information on crack-growth behavior due to internal pressure, and the effect of gas penetration in the radial cracks has also been investigated.

In this section we discuss bench blasting problems based on Outcherlony's setup and the present approach. We solve the problems shown in Figure 6, considering two limiting cases: empty cracks, meaning that no gas pressure penetrates through the radial cracks during blasting; and fully pressurized
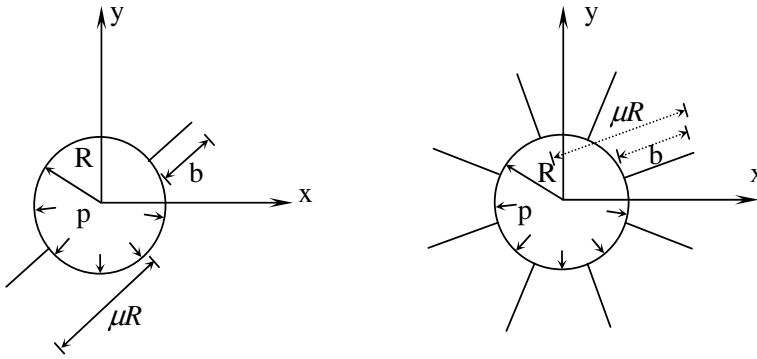
Figure 6. Pressurized circular holes (blast holes) with radial cracks in infinite planes. The examples shown have two (left) and eight (right) radial cracks.

cracks, meaning that the gas pressure fully penetrates the radial cracks, so the gas pressure in the radial cracks equals the total blast hole pressure.

SIDDLCR and SIDDQCR have been used for the numerical solution. The following assumptions and data have used throughout: hole radius, $R = 1$ m; inside pressure, $p = 10$ MPa; modulus of elasticity, $E = 10$ GPa; Poisson's ratio, $\nu = 0.2$; rock fracture toughness, $K_{IC} = 2$ MPa m$^{1/2}$; ratio of crack tip element to crack length, $L/b = 0.1$. Exploiting symmetry, 30 quadratic elements or 40 linear elements are used to discretize the boundary of a circular hole, and 10 quadratic elements or 15 linear elements are used for the discretization of each radial crack (excluding the crack tip elements). We compute numerically the normalized mode-I stress intensity factor $K_I/(p\sqrt{\pi \mu R})$ for different crack length ratios $\mu = (b + R)/R$ of a pressurized blast hole under uniform inside pressure p with 2 and 8 symmetric radial cracks emanating from the hole. These numerical results, for empty and fully pressurized radial cracks, are compared in Figures 7 and 8 with the corresponding analytical values given in [Ouchterlony 1983]. We see that, particularly for long radial cracks, the analytical and numerical values of normalized stress intensity factors (mode-I) are very close to each other. The blasting pressures p are around 0.56 to 1.0 GPa, but the results plotted here are normalized in the form of $K_I/(p\sqrt{\pi \mu R})$.

In a similar manner we analyzed numerically the problem shown in Figure 9 using SIDDQCR. The calculated fracture parameters are shown in Table 6 for the two extreme cases of empty cracks and fully pressurized cracks against different ratios B/R of burden radius to blast hole (B/R can be viewed as a normalized hole depth relative to the free surface of the half-plane). All these results were obtained through SIDDQCR, using a constant value of $\mu = 2.5$ for the crack length ratio.

The analytical results for the problem of a pressurized circular hole with four symmetric empty radial cracks in an infinite plane are: $K_I/(p\sqrt{\pi \mu R}) = 0.1966$ and $K_{II}/(p\sqrt{\pi \mu R}) = 0.0$, and for the fully pressurized radial cracks are: $K_I/(p\sqrt{\pi \mu R}) = 0.9085$ and $K_{II}/(p\sqrt{\pi \mu R}) = 0.0$ respectively [Ouchterlony 1983].

Table 6 compares the different results obtained for the upper crack (the crack near to the free surface of the half-plane), and the lower crack. The results given in this table show that as the burden (B/R ratio) increases the mixed mode stress intensity factors K_I and K_{II} tend to their corresponding analytical values for the infinite plane case.
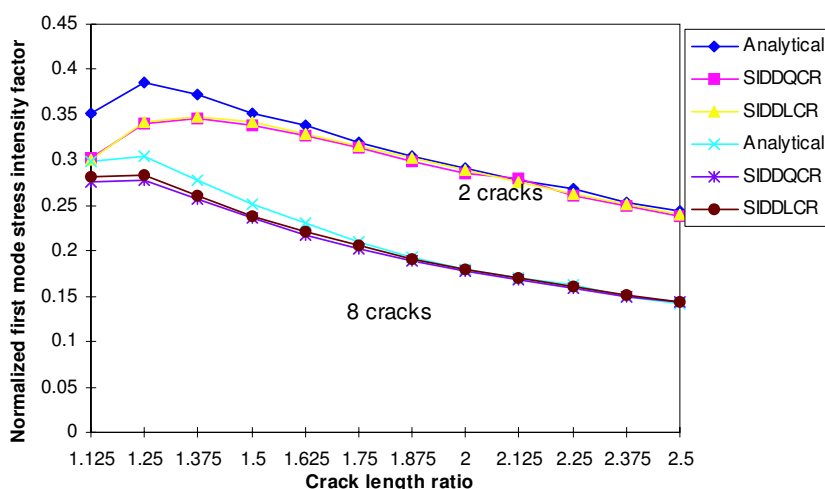
Figure 7. Blast hole with 2 and 8 empty radial cracks: comparison of analytical and numerical values of $K_I/(p\sqrt{\pi\mu R})$ for varying crack length ratio μ.
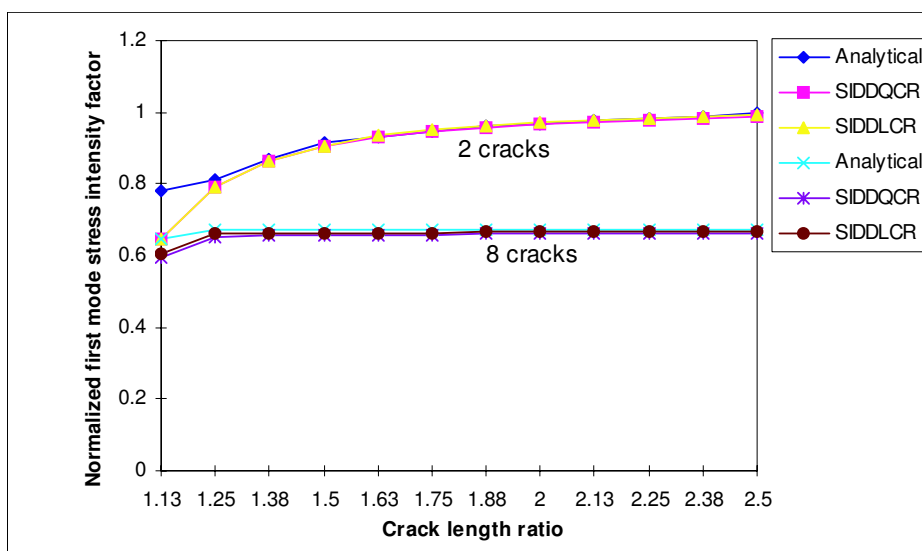

Figure 8. Blast hole with 2 and 8 fully pressurized radial cracks: comparison of analytical and numerical values of $K_I/(p\sqrt{\pi\mu R})$ for varying crack length ratio μ.

The results obtained in this paper show that, as the Mode II stress intensity factor (K_{II}) is very small compared to the Mode I (K_I), and for the practical problems; the crack initiation angle θ_0 is also very small, for both upper and lower cracks, then it may be concluded that the radial cracks produced in blasting operations propagates nearly in their own planes due to the high influence of K_I. However, when the radial cracks become very close to the free surface (that is, for small B/R ratios), the upper cracks divert away from the free surface in the direction of the crack deviation angle θ_0.
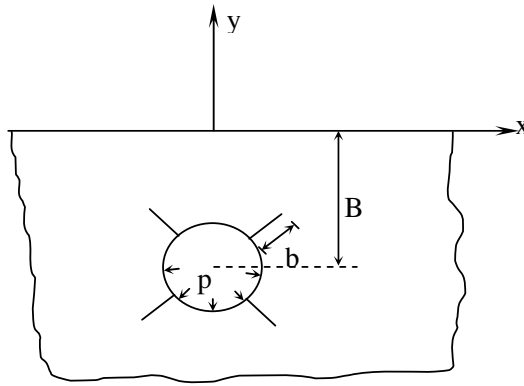
Figure 9. A blast hole in a semi-infinite plane with 4 symmetric radial cracks.

7. Conclusion

The higher-order displacement discontinuity method is used to solve boundary value problems in finite, infinite and semi-infinite plane problems. The special crack tip formulation is also modified and used for solving the crack problems in semi-infinite planes. Then based on the formulation derived in Sections 2 and 3, the two computer programs SIDDLCR (semi-infinite displacement discontinuity method with linear elements for crack analysis) and SIDDQCR (semi-infinite displacement discontinuity method with quadratic elements for crack analysis) were developed. These programs use a special crack tip element

B/R	$K_I/(p\sqrt{\pi\mu R})$		$K_{II}/(p\sqrt{\pi\mu R})$		θ_0 (degrees)	
	Up. crack	Lo. crack	Up. crack	Lo. crack	Up. crack	Lo. crack
2.00	2.2036	1.3534	0.1954	0.0194	−10.0	−1.6
2.25	1.8940	1.2366	0.1230	−0.0307	−7.4	2.8
2.50	1.6993	1.1766	0.1285	−0.0465	−8.6	4.5
2.75	1.5298	1.1352	0.1229	−0.0565	−9.1	5.7
3.00	1.3937	1.1022	0.1109	−0.0626	−9.0	6.5
3.25	1.2690	1.0578	0.0949	−0.0552	−8.5	5.9
3.50	1.1927	1.0392	0.0862	−0.0573	−8.2	6.3
3.75	1.1116	1.0230	0.0609	−0.0587	−6.2	6.5
4.00	1.0344	1.0085	0.0470	−0.0580	−5.5	6.5
4.25	1.0114	0.9960	0.0362	−0.0573	−4.1	6.5
4.50	0.9863	0.9903	0.0223	−0.0523	−2.5	6.0
4.75	0.9582	0.9816	0.0091	−0.0510	−1.1	5.9
5.00	0.9390	0.9745	0.0044	−0.0487	−0.5	5.7

Table 6. Normalized stress intensity factors and crack propagation angle θ_0 for a pressurized hole under uniform inside pressure p, with four fully pressurized radial cracks, for varying values of B/R (corresponding to different depths).

with a simple mixed mode fracture criterion — the maximum tangential stress criterion, based on linear elastic fracture mechanics principles — to quasistatically analyze the radial cracks. For the verification of this method some example problems of cracked bodies in infinite and semi-infinite planes are solved and the results are compared with their existing analytical results and/or with the results obtained by some previous researchers. The computed results obtained by these codes are very accurate as compared to the previous results (given in the literature), which proves the validity and accuracy of the proposed method. For completeness, some of the necessary formulations which are derived and used in these computer codes are also given in the appendices of this paper.

Appendix: Supplementary and image solutions for displacements and stresses

We maintain the notation of Section 2 and Figure 2 and define

$$F_{j8}^I(\bar{x}', \bar{y}') == \frac{\partial^4 F_j^I(\bar{x}', \bar{y}')}{\partial \bar{x}' \partial \bar{y}'^3}, \qquad F_{j9}^I(\bar{x}', \bar{y}') = \frac{\partial^4 F_j^I(\bar{x}', \bar{y}')}{\partial \bar{y}'^4}.$$

The combined displacements $u_i^I + u_i^S$ are

$$
\begin{aligned}
u_x^I + u_x^S = \frac{-1}{4\pi(1-\nu)} \\
\times \sum_{j=1}^{3} \bigg(\Big((1-2\nu)\sin\beta F_{j2}^I - 2(1-\nu)\cos\beta F_{j3}^I + \big((3-4\nu)(y\sin 2\beta - \bar{y}\sin\beta) + 2y\sin 2\beta\big)F_{j4}^I \\
+ \big((3-4\nu)(y\cos 2\beta - \bar{y}\cos\beta) - y(1-2\cos 2\beta)\big)F_{j5}^I \\
+ 2y(y\sin 3\beta - \bar{y}\sin 2\beta)F_{j6}^I - 2y(y\cos 3\beta - \bar{y}\cos 2\beta)F_{j7}^I \Big)D_{\bar{x}}^j \\
+ \Big((1-2\nu)\cos\beta F_{j2}^I + 2(1-\nu)\sin\beta F_{j3}^I - \big((3-4\nu)(y\cos 2\beta - \bar{y}\cos\beta) - y\big)F_{j4}^I \\
+ (3-4\nu)(y\sin 2\beta - \bar{y}\sin\beta)F_{j5}^I \\
- 2y(y\cos 3\beta - \bar{y}\cos 2\beta)F_{j6}^I - 2y(y\sin 3\beta - \bar{y}\sin 2\beta)F_{j7}^I \Big)D_{\bar{y}}^j \bigg),
\end{aligned}
$$

$$
\begin{aligned}
u_y^I + u_y^S = \frac{-1}{4\pi(1-\nu)} \\
\times \sum_{j=1}^{3} \bigg(\Big((1-2\nu)\cos\beta F_{j2}^I - 2(1-\nu)\sin\beta F_{j3}^I - \big((3-4\nu)(y\cos 2\beta - \bar{y}\cos\beta) + y(1-2\cos 2\beta)\big)F_{j4}^I \\
+ \big((3-4\nu)(y\sin 2\beta - \bar{y}\sin\beta) - 2y\sin 2\beta\big)F_{j5}^I \\
+ 2y(y\cos 3\beta - \bar{y}\cos 2\beta)F_{j6}^I + 2y(y\sin 3\beta - \bar{y}\sin 2\beta)F_{j4}^I \Big)D_{\bar{x}}^j \\
+ \Big((1-2\nu)\sin\beta F_{j2}^I - 2(1-\nu)\cos\beta F_{j3}^I - (3-4\nu)(y\sin 2\beta - \bar{y}\sin\beta)F_{j4}^I \\
- \big((3-4\nu)(y\cos 2\beta - \bar{y}\cos\beta) + y\big)F_{j5}^I \\
+ 2y(y\sin 3\beta - \bar{y}\sin 2\beta)F_{j6}^I - 2y(y\cos 3\beta - \bar{y}\cos 2\beta)F_{j7}^I \Big)D_{\bar{y}}^j \bigg),
\end{aligned}
$$

The stresses $\sigma_{ij}^I + \sigma_{ij}^S$ associated with these displacements are

$$\sigma_{xx}^I + \sigma_{xx}^S = \frac{-2G}{4\pi(1-\nu)}$$

$$\left(\left(F_{j4}^I - 3(\cos 2\beta F_{j4}^I - \sin 2\beta)F_{j5}^I + (2y(\cos\beta - 3\cos 3\beta) + 3\bar{y}\cos 2\beta)F_{j6}^I\right.\right.$$
$$+ (2y(\sin\beta - 3\sin 3\beta) + 3\bar{y}\sin 2\beta)F_{j7}^I$$
$$\left. - 2y(y\cos 4\beta - \bar{y}\cos 3\beta)F_{j8}^I - 2y(y\sin 4\beta - \bar{y}\sin 3\beta)F_{j9}^I\right)D_{\bar{x}}^j$$
$$+ \left(F_{j5}^I + (2y(\sin\beta - 2\sin 3\beta) + 3\bar{y}\sin 2\beta)F_{j6}^I - (2y(\cos\beta - 2\cos 3\beta) + 3\bar{y}\cos 2\beta)F_{j7}^I\right.$$
$$\left.\left. - 2y(y\sin 4\beta - \bar{y}\sin 3\beta)F_{j8}^I + 2y(y\cos 4\beta - \bar{y}\cos 3\beta)F_{j9}^I\right)D_{\bar{y}}^j\right),$$

$$\sigma_{yy}^I + \sigma_{yy}^S = \frac{-2G}{4\pi(1-\nu)}$$

$$\left(\left(F_{j4}^I - (\cos 2\beta F_{j4}^I - \sin 2\beta)F_{j5}^I - (4y\sin 2\beta - \bar{y}\cos 2\beta)F_{j6}^I\right.\right.$$
$$\left. + (4y\sin\beta\cos 2\beta + \bar{y}\sin 2\beta)F_{j7}^I + 2y(y\sin 4\beta - \bar{y}\sin 3\beta)F_{j9}^I\right)D_{\bar{x}}^j$$
$$+ \left(F_{j5}^I - (2y\sin\beta - \bar{y}\sin 2\beta)F_{j6}^I + (2y\cos\beta - \bar{y}\cos 2\beta)F_{j7}^I\right.$$
$$\left.\left. + 2y(y\sin 4\beta - \bar{y}\sin 3\beta)F_{j8}^I - 2y(y\cos 4\beta - \bar{y}\cos 3\beta)F_{j9}^I\right)D_{\bar{y}}^j\right),$$

$$\sigma_{xy}^I + \sigma_{xy}^S = \frac{-2G}{4\pi(1-\nu)}$$

$$\left(\left((\sin 2\beta + \cos 2\beta)F_{j4}^I + (2y\sin\beta(1 + 4\cos 2\beta) - \bar{y}\sin 2\beta)F_{j6}^I\right.\right.$$
$$+ (2y\cos\beta(3 - 4\cos 2\beta) + \bar{y}\sin 2\beta)F_{j7}^I$$
$$\left. + 2y(y\sin 4\beta - \bar{y}\sin 3\beta)F_{j8}^I - 2y(y\cos 4\beta - \bar{y}\cos 3\beta)F_{j9}^I\right)D_{\bar{x}}^j$$
$$+ \left((4y\sin\beta\sin 2\beta + \bar{y}\cos 2\beta)F_{j6}^I - (4y\sin\beta\cos 2\beta - \bar{y}\sin 2\beta)F_{j7}^I\right.$$
$$\left.\left. - 2y(y\cos 4\beta - \bar{y}\cos 3\beta)F_{j8}^I - 2y(y\sin 4\beta - \bar{y}\sin 3\beta)F_{j9}^I\right)D_{\bar{y}}^j\right),$$

References

[Aliabadi 1998] M. H. Aliabadi, *Fracture of rocks*, Computational Mechanics Publications, Southampton, 1998.

[Ash 1985] R. L. Ash, "Flexural rapture as a rock breakage mechanism in blasting", pp. 371–378 in *Fragmentation by blasting*, edited by W. L. Fourney et al., Bethel, CT, 1985.

[Backers et al. 2004] T. Backers, G. Dresen, E. Rybacki, and S. O., "New data on mode II fracture toughness of rock from the punch-through shear test", *Int. J. Rock Mech. Min.* **41**:S1 (2004), 2–7. SINOROCK 2004 Symposeum, Paper 1A 01.

[Bobet 2001] A. Bobet, "A hybridized displacement discontinuity method for mixed mode I-II-III loading", *Int. J. Rock Mech. Min.* **38**:8 (2001), 1121–1134.

[Broek 1989] D. Broek, *The practical use of fracture mechanics*, 4th ed., Kluwer, Dordrecht, 1989.

[Carpinteri and Yang 1997] A. Carpinteri and G. Yang, "Size effects in brittle specimen with microcrack interaction", *Comput. Struct.* **63**:3 (1997), 429–437.

[Cho et al. 2004] S. H. Cho, Y. Nakamura, and K. Kaneko, "Dynamic fracture process analysis of rock subjected to a stress wave and gas pressurization", *Int. J. Rock Mech. Min.* **41**:S1 (2004), 433–440. Paper 2A 20, SINOROCK2004 Symposium.

[Courtesen 1979] D. L. Courtesen, "Cavities and gas penetration from blasts in stressed rock with flooded joints", *Acta Astronaut.* **6**:3–4 (1979), 341–363.

[Crawford and Curran 1982] A. M. Crawford and J. H. Curran, "Higher order functional variation displacement discontinuity elements", *Int. J. Rock Mech. Min.* **19**:3 (1982), 143–148.

[Crouch 1976] S. L. Crouch, "Solution of plane elasticity problems by the displacement discontinuity method, I: Infinite body solution", *Int. J. Numer. Methods Eng.* **10**:2 (1976), 301–343.

[Crouch and Starfield 1983] S. L. Crouch and A. M. Starfield, *Boundary element methods in solid mechanics*, Allen and Unwin, London, 1983. MR 84i:73060 Zbl 0528.73083

[Donzé et al. 1997] F. V. Donzé, J. Bouchez, and S. A. Magnier, "Modeling fractures in rock blasting", *Int. J. Rock Mech. Min.* **34**:8 (1997), 1153–1163.

[Erdogan and Sih 1963] F. Erdogan and G. C. Sih, "On the crack extension in plates under plane loading and transverse shear", *J. Basic Eng.* (*ASME*) **85** (1963), 519–527.

[Griffith 1925] A. A. Griffith, "The theory of rupture", pp. 56–63 in *Proceedings of the First International Congress for Applied Mechanics* (Delft, 1924), edited by C. B. Biezeno and J. M. Burgers, Waltman, Delft, 1925.

[Guo et al. 1990] H. Guo, N. I. Aziz, and R. A. Schmidt, "Linear elastic crack tip modeling by the displacement discontinuity method", *Eng. Fract. Mech.* **36**:6 (1990), 933–943.

[Guo et al. 1992] H. Guo, N. I. Aziz, and R. A. Schmidt, "Rock cutting study using linear elastic fracture mechanics", *Eng. Fract. Mech.* **41**:5 (1992), 771–778.

[Huang and Wang 1985] J.-A. Huang and S. Wang, "An experimental investigation concerning the comprehensive fracture toughness of some brittle rocks", *Int. J. Rock Mech. Min.* **22**:2 (1985), 99–104.

[Ingraffea 1981] A. R. Ingraffea, "Mixed-mode fracture initiation in Indiana sandstone and Westerly granite", pp. 199–204 in *Rock mechanics from research to application: proceedings of the 22nd US Symposium on Rock Mechanics* (MIT), edited by H. H. Einstein, MIT, Cambridge, MA, 1981.

[Ingraffea 1983] A. R. Ingraffea, "Numerical modeling of fracture propagation", pp. 151–208 in *Rock fracture mechanics*, edited by H. P. Rossmanith, Courses and Lectures / International Centre for Mechanical Sciences **275**, Springer, Vienna, 1983.

[Ingraffea 1987] A. R. Ingraffea, "Theory of crack initiation and propagation in rock", pp. 71–110 in *Fracture mechanics of rock*, edited by B. K. Atkinson, Academy Press, London, 1987.

[Kutter and Fairhurst 1971] H. K. Kutter and C. Fairhurst, "On the fracture process in blasting", *Int. J. Rock Mech. Min.* **8**:3 (1971), 181–188.

[Mortazavi and Katsabanis 2001] A. Mortazavi and P. D. Katsabanis, "Modeling burden size and strata dip effects on surface blasting process", *Int. J. Rock Mech. Min.* **38** (2001), 481–498.

[Ouchterlony 1983] F. Ouchterlony, "Analysis of cracks", pp. 31–67 in *Rock fracture mechanics*, edited by H. P. Rossmanith, Springer, Vienna, 1983.

[Ouchterlony 1988] F. Ouchterlony, "Suggested methods for determining the fracture toughness of rock: ISRM commission on testing methods", *Int. J. Rock Mech. Min.* **25**:2 (1988), 71–96.

[Rao et al. 2003] Q. Rao, Z. Sun, O. Stephansson, C. Li, and B. Stillborg, "Shear fracture (mode II) of brittle rock", *Int. J. Rock Mech. Min.* **40**:3 (2003), 355–375.

[Rossmanith 1983] H. P. Rossmanith, *Rock fracture mechanics*, Springer, New York, 1983.

[Scavia 1992] C. Scavia, "A numerical technique for the analysis of cracks subjected to normal compressive stresses", *Int. J. Numer. Methods Eng.* **33**:5 (1992), 929–942.

[Scavia 1995] C. Scavia, "A method for the study of crack propagation in rock structures", *Géotechnique* **45** (1995), 447–463.

[Shen et al. 2004] B. Shen, O. Stephansson, M. Rinne, H.-S. Lee, L. Jing, and K. Roshoff, "A fracture propagation code and its application to nuclear waste disposal", *Int. J. Rock Mech. Min.* **41**:S1 (2004), 472–477.

[Shou and Crouch 1995] K. J. Shou and S. L. Crouch, "A higher order displacement discontinuity method for analysis of crack problems", *Int. J. Rock Mech. Min.* **32**:1 (1995), 49–55.

[Stephansson 2002] O. Stephansson, "Recent rock fracture mechanics developments", pp. 37–60 in *Proceedings of the First Iranian Rock Mechanics Conference* (Tehran), 2002.

[Stephansson et al. 2001] O. Stephansson, T. Backers, G. Dresen, and E. Rybacki, "Shear fracture mechanics of rocks and a new testing method for K_{IIC}", pp. 163–168 in *Rock mechanics: a challenge for society: proceedings of the ISRM Regional Symposium: EUROCK 2001* (Espoo, Finland), edited by P. Sarkka and P. Eloranta, Taylor and Francis, London, 2001.

[Tan et al. 1996] X. C. Tan, S. Q. Kou, and P. A. Lindqvist, *Simulation of rock fragmentation by indenters using DDM and fracture mechanics*, edited by M. Aubertin et al., A. A. Balkema, Rotterdam, 1996.

[Whittaker et al. 1992] B. N. Whittaker, R. N. Singh, and G. Sun, *Rock fracture mechanics: principles, design and applications*, Developments in Geotechnical Engineering **71**, Elsevier, Amsterdam, 1992.

[Zipf and Bieniawski 1989] R. K. Zipf and Z. T. Bieniawski, "Development of the mixed mode testing system for geological materials", pp. 338–352 in *Fracture of concrete and rock: SEM-RILEM International Conference* (Houston, TX, 1987), edited by S. P. Shah and S. E. Swartz, Springer, New York, 1989.

HASAN HOSSEINI_NASAB: hhn@yazduni.ac.ir
Industrial Engineering Department, Engineering Faculty, Yazd University, Safaiyeh, Yazd, Iran

MOHAMMAD FATEHI MARJI: mfatehi@yazduni.ac.ir
Mining Engineering Department, Engineering Faculty, Yazd University, Safaiyeh, Yazd, Iran